JOURNAL OF BIOMEDICAL OPTICS 2(3), 282–294 (JULY 1997)

INTEGRAL EQUATION SOLUTION TO THE SCATTERING OF ELECTROMAGNETIC RADIATION BY A SYSTEM OF TWO INTERACTING TRIAXIAL DIELECTRIC ELLIPSOIDS: THE CASE OF A TWO RED BLOOD CELL ROULEAU

Georgios S. Stamatakos,[†] Nikolaos K. Uzunoglu,[‡] and Dido Yova[‡]
[†]National Technical University of Athens, Department of Physics, Zografou Campus, GR-157 80 Athens, Greece; [‡]National Technical University of Athens, Division of Electroscience, Department of Electrical and Computer Engineering, Zografou Campus, GR-157 80 Athens, Greece

(Paper JBO-121 received Nov. 5, 1996; revised manuscript received Apr. 22, 1997; accepted for publication May 5, 1997.)

ABSTRACT

A mathematical formulation of the problem of electromagnetic wave scattering by a system of two homogeneous triaxial dielectric ellipsoids of complex index of refraction is presented. The analysis is based on the Lippman–Schwinger integral equation for an electric field. The corresponding integral equation for the scattering, which contains two singular kernels, is transformed into a pair of nonsingular integral equations for the angular Fourier transform of the electric field inside each scatterer. The latter equations are solved by reducing them by quadrature into a matrix equation. The resulting solutions are used to calculate the scattering amplitude. As a numerical application, the case of a two red blood cell rouleau model is considered. Typical values of the appropriate discretization parameters, which proved sufficient for achieving convergence, are presented, along with validity tests. The effect of the electromagnetic coupling of the scatterers is also illustrated. Efficient techniques, which are capable of reducing the rather high computing demands of the analysis, such as parallel processing, are both suggested and applied. © *1997 Society of Photo-Optical Instrumentation Engineers.* [S1083-3668(97)00503-0]

Keywords electromagnetic scattering; dielectric ellipsoids; red blood cells; aggregation.

1 INTRODUCTION

The problem of electromagnetic scattering by a system of two interacting dielectric ellipsoids has been rigorously solved only for special forms of the general triaxial ellipsoid. Examples include electromagnetic scattering by a pair of spheres[1–3] and by a pair of prolate spheroids.[4]

In this paper, a solution to the problem of electromagnetic scattering by a system of two uniformly lossy general dielectric triaxial ellipsoids is presented. The shape of a triaxial ellipsoid is highly versatile and consequently can be used to model a large number of scattering objects [e.g, raindrops, airplanes, fish, tumors, erythrocytes (normal, pathological, deformed, and aggregated)]. In the biomedical field, our approach may be of particular interest to the study of the aggregation of elliptocytes. Elliptocytes are abnormal erythrocytes that have a shape close to a triaxial ellipsoid (discoidal elliptocytes). They are present in many forms of anemia (e.g., hereditary elliptocytosis, thalassemia, and megaloblastic anemias) in varying proportions. In hereditary elliptocytosis, they may constitute up to 98% of the total number of erythrocytes.[5]

A Fredholm integral equation model (FIEM) is developed, based on the Lippman–Schwinger integral equation for the electric field. However, the corresponding integral equation for the scattering contains two singular kernels. Therefore, it is transformed into a pair of nonsingular integral equations for the angular Fourier transform of the electric field inside each ellipsoid. The latter equations are solved by reducing them by quadrature into a matrix equation. The resulting solutions are used to calculate the scattering amplitude.

Serial and parallel computer codes have been developed and run on various Silicon Graphics International Inc. (SGI) shared-memory parallel systems.

Address all correspondence to Nikolaos Uzunoglu, Tel: 301 772 3556; Fax: 301 772 3557; E-mail: nuzu@central.ntua.gr

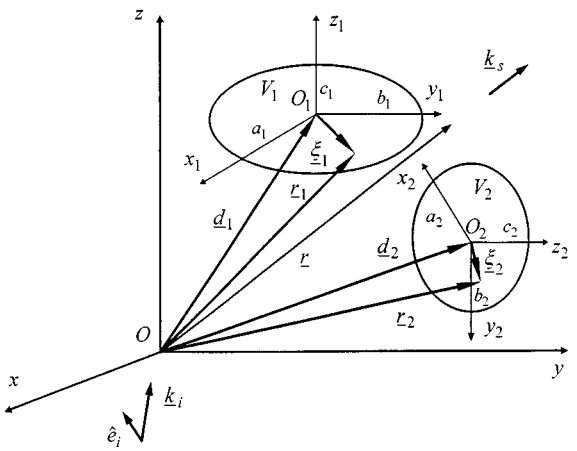

Fig. 1 Geometry of the problem.

The convergence of the complete model has been checked for the case of plane wave irradiation ($\lambda = 0.633\ \mu$m in vacuum) of a system of two adjacent oblate spheroidal models of erythrocytes. Two different angles of incidence have been considered.

A partial test of the computer code has been performed by comparing the scattering diagram of a single spherical erythrocyte irradiated by red light ($\lambda = 0.633\ \mu$m in vacuum) as predicted by FIEM with the diagram predicted by Mie theory. A further test ensuring the validity of the analysis for the approximate case with the electromagnetic interaction neglected has also been applied. The effect of electromagnetic coupling between two adjacent erythrocytes is illustrated. It is demonstrated that the near-forward scattering pattern allows easy discrimination between a single red blood cell (RBC) and a RBC doublet (e.g., in flow cytometry). Typical values of the discretization parameters present in FIEM that are sufficient for obtaining convergence are provided.

2 THEORY

2.1 THE MODEL

Both RBCs (or dielectric scatterers in general) are modeled as triaxial homogeneous dielectric ellipsoids with semiaxes a_1, b_1, c_1 and a_2, b_2, c_2, respectively (Figure 1). For $a_1 = b_1$, $c_1 < a_1$ and $a_2 = b_2$, $c_2 < a_2$, the shapes of oblate spheroids, which are relatively close to the shapes of normal discoid RBCs, are obtained. For $a_1 = b_1$, $c_1 > a_1$ and $a_2 = b_2$, $c_2 > a_2$, the shapes of prolate spheroids which can model mechanically deformed RBCs are obtained. The relative (to the suspending medium) index of refraction n_0 and consequently the relative dielectric constant $\epsilon = n_0^2$ of both RBCs for a given wavelength are considered to be complex. The index of refraction of the suspending medium, which is usually plasma or an optically eqivalent isotonic liquid, is considered real. Plasma has a very low optical absorption in the visible spectrum range, where most diagnostic instruments operate.

Dyadic notation is used throughout the analysis. The following three cartesian coordinate systems are used: the ''absolute'' system xyz and the local coordinate systems $x_1y_1z_1$ and $x_2y_2z_2$ with their origins at the centers of the ellipsoids V_1 and V_2, respectively (Figure 1). The ellipsoids V_m, $m = 1,2$ are defined in their corresponding local coordinate systems by the equation

$$\frac{x_m^2}{a_m^2} + \frac{y_m^2}{b_m^2} + \frac{z_m^2}{c_m^2} = 1. \tag{1}$$

The following symbol conventions are used throughout the analysis. X denotes a scalar quantity (generally a complex number). $\underline{X}$, $\underline{\underline{X}}$ denote vectors (generally of complex elements). $\hat{X}$, $\hat{\underline{X}}$, $\hat{\underline{\underline{X}}}$ denote unit vectors (of real elements). $\bar{\underline{X}}$ denotes a matrix or a dyadic (generally of complex elements). A product sign at the beginning of an equation continuation line stands for a scalar product.

A plane electromagnetic wave of wave vector $\underline{k}_i = k_0 \hat{k}_i$ and polarization $\hat{e}_i$ is incident on the system of the two ellipsoids. The time dependence is taken as $\exp(-i\omega t)$ and is suppressed throughout the analysis. The electric field (dyadic) at any point $\underline{r}$ in the xyz coordinate system is given by[6–8]

$$\bar{\underline{E}}(\underline{r}) = \bar{\underline{J}}_i \exp(i\underline{k}_i \cdot \underline{r}) + \int_{V_1} d\underline{r}_1 \gamma \bar{\underline{G}}(\underline{r}, \underline{r}_1) \cdot \bar{\underline{E}}(\underline{r}_1) + \int_{V_2} d\underline{r}_2 \gamma \bar{\underline{G}}(\underline{r}, \underline{r}_2) \cdot \bar{\underline{E}}(\underline{r}_2), \tag{2}$$

where

$$\gamma = \frac{k_0^2}{4\pi}(\epsilon - 1), \tag{3}$$

k_0 is the suspending medium propagation constant, $\bar{\underline{1}}$ is the unit dyadic,

$$\bar{\underline{J}}_\lambda = \bar{\underline{1}} - \hat{\underline{k}}_\lambda \hat{\underline{k}}_\lambda \quad \text{for any subscript } \lambda, \tag{4}$$

$\hat{\underline{k}}_\lambda$ is a unit vector along $\underline{k}_\lambda$,

$$\bar{\underline{G}}(\underline{r}, \underline{r}_m) = (\bar{\underline{1}} + k_0^{-2} \nabla\nabla) G(\underline{r}, \underline{r}_m), \quad m = 1,2 \tag{5}$$

and

$$G(\underline{r}, \underline{r}_m) = \frac{\exp(ik_0 |\underline{r} - \underline{r}_m|)}{|\underline{r} - \underline{r}_m|}. \tag{6}$$

In order to obtain the plane plus scattered wave for an incident wave $\hat{e}_i E_0 \exp(i\underline{k}_i \cdot \underline{r})$, both sides of (2) should be multiplied by $\hat{e}_i E_0$.

If the vectors ξ_1 and ξ_2 (Figure 1) are expressed in the local coordinate systems $x_1y_1z_1$ and $x_2y_2z_2$ respectively, the following relations hold

$$\underline{r}_1=\underline{d}_1+\bar{\underline{A}}_1\cdot\underline{\xi}_1, \tag{7}$$

$$d\underline{r}_1=d\underline{\xi}_1, \tag{8}$$

$$\underline{r}_2=\underline{d}_2+\bar{\underline{A}}_2\cdot\underline{\xi}_2 \tag{9}$$

and

$$d\underline{r}_2=d\underline{\xi}_2. \tag{10}$$

The xyz coordinate system may be considered as originating from either the $x_1y_1z_1$ or the $x_2y_2z_2$ local system by rotation and translation as follows. The $x_1y_1z_1$ system is rotated (counterclockwise) about its original z_1 axis by the ψ_1 angle ($0\leq\psi_1\leq 2\pi$); the transformed system is rotated about its new y_1 axis by the θ_1 angle ($-\pi/2\leq\vartheta_1\leq\pi/2$), and the latter system is rotated about its new x_1 axis by the ω_1 angle ($0\leq\omega_1\leq 2\pi$). The emerged system is translated by the vector $-\underline{d}_1$ so that the xyz coordinate system is obtained. Similarly, the absolute xyz system may be obtained from the local $x_2y_2z_2$ coordinate system (Euler angles ψ_2, ϑ_2 and ω_2, translation vector $-\underline{d}_2$). Then the matrix $\bar{\underline{A}}_1$ is given by[9]

$$\bar{\underline{A}}_1=\begin{bmatrix}\cos(\psi_1)\cos(\theta_1) & \sin(\psi_1)\cos(\vartheta_1) & -\sin(\vartheta_1)\\ [-\sin(\psi_1)\cos(\omega_1) & [\cos(\psi_1)\cos(\omega_1) & \\ +\cos(\psi_1)\sin(\theta_1)\sin(\omega_1)] & +\sin(\psi_1)\sin(\vartheta_1)\sin(\omega_1)] & \cos(\vartheta_1)\sin(\omega_1)\\ [\sin(\psi_1)\sin(\omega_1) & [-\cos(\psi_1)\sin(\omega_1) & \\ +\cos(\psi_1)\sin(\vartheta_1)\cos(\omega_1)] & +\sin(\psi_1)\sin(\vartheta_1)\cos(\omega_1)] & \cos(\vartheta_1)\cos(\omega_1)\end{bmatrix}. \tag{11}$$

The matrix $\bar{\underline{A}}_2$ is given by Eq. (11) if all 1 subscripts are substituted for by 2 subscripts.

The dyadic scattering amplitude $\bar{\underline{f}}(\underline{k}_s,\underline{k}_i)$ for scattering in the direction of $\underline{k}_s=k_0\hat{\underline{k}}_s$ is defined by[10]

$$\bar{\underline{E}}(\underline{r})\xrightarrow[r\to\infty]{}\bar{\underline{J}}_i\exp(ik\underline{k}_i\cdot\underline{r})+\frac{\exp(ik_0r)}{r}\bar{\underline{f}}(\underline{k}_s,\underline{k}_i)+0\left(\frac{1}{r^2}\right), \tag{12}$$

where $r=|\underline{r}|$.

Considering the asymptotic form of (2) as $r\to\infty$ gives

$$\lim_{|\underline{r}|\to\infty}\bar{\underline{E}}(\underline{r})=\bar{\underline{J}}_i\exp(ik\underline{k}_i\cdot\underline{r})+\frac{\exp(ik_0r)}{r}\times\bar{\underline{J}}_s\cdot\left[\int_{V_1}\gamma\exp(-ik\underline{k}_s\cdot\underline{r}_1)\bar{\underline{E}}(\underline{r}_1)d\underline{r}_1+\int_{V_2}\gamma\exp(-ik\underline{k}_s\cdot\underline{r}_2)\bar{\underline{E}}(\underline{r}_2)d\underline{r}_2\right]. \tag{13}$$

Therefore, the dyadic scattering amplitude is expressed as

$$\bar{\underline{f}}(\underline{k}_s,\underline{k}_i)=\bar{\underline{J}}_s\cdot\left[\int_{V_1}\gamma\exp(-ik\underline{k}_s\cdot\underline{r}_1)\bar{\underline{E}}(\underline{r}_1)d\underline{r}_1+\int_{V_2}\gamma\exp(-ik\underline{k}_s\cdot\underline{r}_2)\bar{\underline{E}}(\underline{r}_2)d\underline{r}_2\right], \tag{14}$$

and the vector scattering amplitude for incident wave polarization $\hat{e}_i$ is given by

$$\underline{f}(\underline{k}_s,\underline{k}_i,e_i)=\bar{\underline{f}}(\underline{k}_s,\underline{k}_i)\cdot\hat{e}_i. \tag{15}$$

2.2 METHOD OF SOLUTION

The field equation (2) is an integral equation with two singular kernels. In what follows, a method is applied that deals with the singularity analytically, leaving two integral equations with nonsingular kernels. Multiplying (2) by $(\gamma/k_0^2)\exp(-ik\underline{k}_1\cdot\underline{r})$ (where $\underline{k}_1=k_1\hat{\underline{k}}_1$ is at present an arbitrary vector) and integrating throughout the volume of the scatterer V_1 gives

$$\frac{1}{k_0^2}\int_{V_1}\gamma\exp(-ik\underline{k}_1\cdot\underline{r})\bar{\underline{E}}(\underline{r})d\underline{r}=\bar{\underline{J}}_i\frac{1}{k_0^2}\int_{V_1}\gamma\exp[(\underline{k}_i-\underline{k}_1)\cdot\underline{r}]d\underline{r}+\frac{1}{k_0^2}\int_{V_1}d\underline{r}\,\gamma\times\exp(-ik\underline{k}_1\cdot\underline{r})\int_{V_1}d\underline{r}_1\gamma\bar{\underline{G}}(\underline{r},\underline{r}_1)\cdot\bar{\underline{E}}(\underline{r}_1)+\frac{1}{k_0^2}\times\int_{V_1}d\underline{r}\,\gamma\exp(-ik\underline{k}_1\cdot\underline{r})\int_{V_2}d\underline{r}_2\gamma\bar{\underline{G}}(\underline{r},\underline{r}_2)\cdot\bar{\underline{E}}(\underline{r}_2). \tag{16}$$

The electric field inside each scatterer V_m, $m=1,2$ is expressed as the Fourier transform (in the xyz coordinate system)

$$\underline{\bar{E}}(\underline{r}_m)=\int d\underline{k}_2\underline{\bar{C}}_m(\underline{k}_2)\exp(i\underline{k}_2\cdot\underline{r}_m)\quad m=1,2, \tag{17}$$

where

$$\underline{k}_2=k_2\hat{k}_2. \tag{18}$$

Substituting (17) into (16) gives

$$\int d\underline{k}_2(\underline{\bar{K}}^{aa}(\underline{k}_1,\underline{k}_2)\ \ \underline{\bar{K}}^{ab}(\underline{k}_1,\underline{k}_2))\begin{pmatrix}\bar{C}_1(\underline{k}_2)\\ \bar{C}_2(\underline{k}_2)\end{pmatrix}$$
$$=\underline{\bar{J}}_i U_{V_1}(\underline{k}_1,\underline{k}_i)\ \text{ for any }\ \underline{k}_1, \tag{19}$$

where

$$U_{V_1}(\underline{k}_1,\underline{k}_2)=\frac{1}{k_0^2}\int_{V_1}\gamma\exp[-i(\underline{k}_1-\underline{k}_2)\cdot\underline{r}_1]d\underline{r}_1\ \text{ for any }\ \underline{k}_1,\underline{k}_2 \tag{20}$$

$$\underline{\bar{K}}^{aa}(\underline{k}_1,\underline{k}_2)=\underline{\bar{1}}U_{V_1}(\underline{k}_1,\underline{k}_2)-\frac{1}{k_0^2}\int_{V_1}d\underline{r}'_1\int_{V_1}d\underline{r}_1\gamma\times\exp(-i\underline{k}_1\cdot\underline{r}'_1)\underline{\bar{G}}(\underline{r}'_1,\underline{r}_1)\gamma\times\exp(i\underline{k}_2\cdot\underline{r}_1), \tag{21}$$

and

$$\underline{\bar{K}}^{ab}(\underline{k}_1,\underline{k}_2)=-\frac{1}{k_0^2}\int_{V_1}d\underline{r}_1\int_{V_2}d\underline{r}_2\gamma\exp(-i\underline{k}_1\cdot\underline{r}_1)\times\underline{\bar{G}}(\underline{r}_1,\underline{r}_2)\gamma\exp(i\underline{k}_2\cdot\underline{r}_2). \tag{22}$$

Now multiplying (2) by $(\gamma/k_0^2)\exp(-i\underline{k}_1\cdot\underline{r})$, integrating throughout the volume of the second scatterer V_2, and substituting (17) into the resulting equation gives

$$\int d\underline{k}_2[\underline{\bar{K}}^{ba}(\underline{k}_1,\underline{k}_2)\underline{\bar{K}}^{bb}(\underline{k}_1,\underline{k}_2)]\begin{bmatrix}\bar{C}_1(\underline{k}_2)\\ \bar{C}_2(\underline{k}_2)\end{bmatrix}$$
$$=\underline{\bar{J}}_i U_{V_2}(\underline{k}_1,\underline{k}_i)\ \text{ for any }\ \underline{k}_1, \tag{23}$$

where

$$U_{V_2}(\underline{k}_1,\underline{k}_2)=\frac{1}{k_0^2}\int_{V_2}\gamma\exp[-i(\underline{k}_1-\underline{k}_2)\cdot\underline{r}_2]d\underline{r}_2, \tag{24}$$

$$\underline{\bar{K}}^{ba}(\underline{k}_1,\underline{k}_2)=-\frac{1}{k_0^2}\int_{V_2}d\underline{r}_2\int_{V_1}d\underline{r}_1\gamma\times\exp(-i\underline{k}_1\cdot\underline{r}_2)\underline{\bar{G}}(\underline{r}_2,\underline{r}_1)\gamma\exp(i\underline{k}_2\cdot\underline{r}_1) \tag{25}$$

and

$$\underline{\bar{K}}^{bb}(\underline{k}_1,\underline{k}_2)=\underline{\bar{1}}U_{V_2}(\underline{k}_1,\underline{k}_2)-\frac{1}{k_0^2}\int_{V_2}d\underline{r}'_2\int_{V_2}d\underline{r}_2\gamma\times\exp(-i\underline{k}_1\cdot\underline{r}'_2)\underline{\bar{G}}(\underline{r}'_2,\underline{r}_2)\gamma\times\exp(i\underline{k}_2\cdot\underline{r}_2). \tag{26}$$

Combining (19) and (23) gives

$$\int d\underline{k}_2\begin{bmatrix}\underline{\bar{K}}^{aa}(\underline{k}_1,\underline{k}_2) & \underline{\bar{K}}^{ab}(\underline{k}_1,\underline{k}_2)\\ \underline{\bar{K}}^{ba}(\underline{k}_1,\underline{k}_2) & \underline{\bar{K}}^{bb}(\underline{k}_1,\underline{k}_2)\end{bmatrix}\begin{bmatrix}\bar{C}_1(\underline{k}_2)\\ \bar{C}_2(\underline{k}_2)\end{bmatrix}=\begin{bmatrix}\underline{\bar{J}}_i U_{V_1}(\underline{k}_1,\underline{k}_i)\\ \underline{\bar{J}}_i U_{V_2}(\underline{k}_1,\underline{k}_i)\end{bmatrix}\ \text{ for any }\ \underline{k}_1. \tag{27}$$

Using the transform

$$\frac{\exp(ik_0|\underline{r}-\underline{r}'|)}{|\underline{r}-\underline{r}'|}=\frac{1}{2\pi^2}\lim_{\epsilon'\to 0^+}\int\frac{d\underline{p}}{p^2-k_0^2-i\epsilon'}\exp[i\underline{p}\cdot(\underline{r}-\underline{r}')] \tag{28}$$

and the dyadic relations

$$k_0^2\underline{\bar{G}}(\underline{r},\underline{r}')=-\underline{\bar{1}}4\pi\delta(\underline{r}-\underline{r}')+\nabla\times\left\{\nabla\times\underline{\bar{1}}\frac{\exp(ik_0|\underline{r}-\underline{r}'|)}{|\underline{r}-\underline{r}'|}\right\} \tag{29}$$

and

$$\nabla\times\nabla\times\underline{\bar{1}}G(\underline{r},\underline{r}')=(\nabla\nabla-\nabla^2\underline{\bar{1}})G(\underline{r},\underline{r}'), \tag{30}$$

Eq. (21) gives

$$\underline{\bar{K}}^{aa}(\underline{k}_1,\underline{k}_2)=\epsilon\underline{\bar{1}}U_{V_1}(\underline{k}_1,\underline{k}_2)-\frac{1}{2\pi^2}\lim_{\epsilon'\to 0^+}\int\frac{d\underline{p}}{p^2-k_0^2-i\epsilon'}\,p^2(\underline{\bar{1}}-\hat{p}\hat{p})\times U_{V_1}(\underline{k}_1,\underline{p})U_{V_1}(\underline{p},\underline{k}_2). \tag{31}$$

Substituting Eqs. (7) and (8) into (20) gives

$$U_{V_1}(\underline{k}_1,\underline{k}_2)=\exp[-i(\underline{k}_1-\underline{k}_2)\cdot\underline{d}_1]U'_{V_1}(\underline{K}_{11},\underline{K}_{21}), \tag{32}$$

where

$$U'_{V_1}(\underline{K}_{11},\underline{K}_{21})=\int_{V_1}d\xi_1\frac{\gamma}{k_0^2}\exp[-i(\underline{K}_{11}-\underline{K}_{21})\cdot\xi_1], \tag{33}$$

$$\underline{K}_{11}=\underline{k}_1\cdot\underline{\bar{A}}_1 \tag{34}$$

and

$$\underline{K}_{21}=\underline{k}_2\cdot\underline{\bar{A}}_1. \tag{35}$$

Similarly,

$$U_{V_1}(\underline{k}_1,\underline{p})=\exp[-i(\underline{k}_1-\underline{p})\cdot\underline{d}_1]U'_{V_1}(\underline{K}_{11},\underline{P}_1), \tag{36}$$

where

$$U'_{V_1}(\underline{K}_{11},\underline{P}_1)=\int_{V_1} d\underline{\xi}_1\ \frac{\gamma}{k_0^2}\ \exp[-i(\underline{K}_{11}-\underline{P}_1)\cdot\underline{\xi}_1], \tag{37}$$

$$\underline{P}_1=\underline{p}\cdot\underline{\bar{A}}_1 \tag{38}$$

and

$$U_{V_1}(\underline{p},\underline{k}_2)=\exp[-i(\underline{p}-\underline{k}_2)\cdot\underline{d}_1]U'_{V_1}(\underline{P}_1,\underline{K}_{21}), \tag{39}$$

where

$$U'_{V_1}(\underline{P}_1,\underline{K}_{21})=\int_{V_1} d\underline{\xi}_1\ \frac{\gamma}{k_0^2}\ \exp[-i(\underline{P}_1-\underline{K}_{21})\cdot\underline{\xi}_1]. \tag{40}$$

The $\underline{K}_{11}$, $\underline{K}_{21}$, and $\underline{P}_1$ vectors are expressed in the local coordinate system $x_1y_1z_1$. Using (32), (36), and (39), Eq. (31) becomes

$$\begin{aligned}\bar{\underline{K}}^{aa}(\underline{k}_1,\underline{k}_2)=\epsilon\bar{\underline{1}}\ &\exp[-i(\underline{k}_1-\underline{k}_2)\cdot\underline{d}_1]U'_{V_1}(\underline{K}_{11},\underline{K}_{21})\\ &-\frac{1}{2\pi^2}\lim_{\epsilon'\to 0^+}\int\frac{d\underline{p}p^2}{p^2-k_0^2-i\epsilon'}\\ &\times(\bar{\underline{1}}-\hat{p}\hat{p})\exp[-i(\underline{k}_1-\underline{p})\\ &\cdot\underline{d}_1]U'_{V_1}(\underline{K}_{11},\underline{P}_1)\exp[-i(\underline{p}-\underline{k}_2)\\ &\cdot\underline{d}_1]U'_{V_1}(\underline{P}_1,\underline{K}_{21}).\end{aligned} \tag{41}$$

Recall that the ellipsoid V_1 is defined by (1) in the local coordinate system $x_1y_1z_1$. The evaluation of $U'_{V_1}(\underline{K}_{11},\underline{K}_{21})$ (otherwise known as the first Born term) is straightforward and we give the result only:

$$U'_{V_1}(\underline{K}_{11},\underline{K}_{21})=a_1b_1c_1(\epsilon-1)\ \frac{j_1(|\underline{K}_{11}-\underline{K}_{21}|_c)}{|\underline{K}_{11}-\underline{K}_{21}|_c}, \tag{42}$$

for any free vectors $\underline{K}_{11}$ and $\underline{K}_{21}$, where

$$\begin{aligned}\underline{K}_{11}&=k_1(\sqrt{1-x_{k_1}^2}\cos\varphi_{k_1},\sqrt{1-x_{k_1}^2}\sin\varphi_{k_1},x_{k_1})\cdot\underline{\bar{A}}_1\\ &\equiv k_1(H_x,H_y,H_z),\end{aligned} \tag{43}$$

(k_1 can take complex values),

$$x_a=\cos(\vartheta_a)\ \text{ for any subscript } a, \tag{44}$$

$$\underline{\underline{K}}_{11}=k_1(a_1H_x,b_1H_y,c_1H_z), \tag{45}$$

$$\begin{aligned}\underline{K}_{21}&=k_2(\sqrt{1-x_{k_2}^2}\cos\varphi_{k_2},\sqrt{1-x_{k_2}^2}\sin\varphi_{k_2},x_{k_2})\cdot\underline{\bar{A}}_1\\ &\equiv k_2(\Lambda_x,\Lambda_y,\Lambda_z)\end{aligned} \tag{46}$$

and

$$\hat{\underline{\underline{K}}}_{21}=k_2(a_1\Lambda_x,b_1\Lambda_y,c_1\Lambda_z), \tag{47}$$

(k_2 can take complex values). For homogeneous scatterers

$$k_1=k_2=k_0n_0. \tag{48}$$

The symbol $|\ |_c$ is defined by the relation

$$|\underline{A}-\underline{B}|_c=\sqrt{A^2+B^2-2\underline{A}\cdot\underline{B}}, \tag{49}$$

where

$$\underline{A}=A\hat{A} \tag{50}$$

and

$$\underline{B}=B\hat{B} \tag{51}$$

(A,B are generally complex numbers). The symbol $\sqrt{z}=[r\exp(i\varphi)]^{1/2}$ denotes the complex square root $r^{1/2}\exp(i\,\varphi/2)$ and $j_n(z)$ is the complex spherical Bessel function of order n.

Thus, (41) takes the form

$$\begin{aligned}\bar{\underline{K}}^{aa}(\underline{k}_1,\underline{k}_2)=\exp[-i(\underline{k}_1-\underline{k}_2)\cdot\underline{d}_1]\Bigg[&\epsilon\bar{\underline{1}}a_1b_1c_1(\epsilon-1)\\ &\times\frac{j_1(|\underline{\underline{K}}_{11}-\underline{\underline{K}}_{21}|_c)}{|\underline{\underline{K}}_{11}-\underline{\underline{K}}_{21}|_c}\\ &-\frac{1}{2\pi^2}\ (a_1b_1c_1)^2(\epsilon-1)^2\\ &\times\lim_{\epsilon'\to 0^+}\int\frac{d\underline{p}p^2}{p^2-k_0^2-i\epsilon'}\ (\bar{\underline{1}}-\hat{p}\hat{p})\\ &\times\frac{j_1(|\underline{\underline{K}}_{11}-\underline{\underline{P}}_1|_c)}{|\underline{\underline{K}}_{11}-\underline{\underline{P}}_1|_c}\frac{j_1(|\underline{\underline{P}}_1-\underline{\underline{K}}_{21}|_c)}{|\underline{\underline{P}}_1-\underline{\underline{K}}_{21}|_c}\Bigg],\end{aligned} \tag{52}$$

where

$$\begin{aligned}\underline{P}_1&=p(\sqrt{1-x_p^2}\cos\varphi_p,\sqrt{1-x_p^2}\sin\varphi_p,x_p)\cdot\underline{\bar{A}}_1\\ &\equiv p(Z_x,Z_y,Z_z)\end{aligned} \tag{53}$$

and

$$\underline{\underline{P}}_1=p(a_1Z_x,b_1Z_y,c_1Z_z). \tag{54}$$

We use the expansion[11]

$$\begin{aligned}\frac{j_1(|\underline{r}_1-\underline{r}_2|_c)}{|\underline{r}_1-\underline{r}_2|_c}=&\sum_{n=0}^{+\infty}(2n+3)\\ &\times\frac{j_{n+1}(|\underline{r}_1|_c)}{|\underline{r}_1|_c}\frac{j_{n+1}(|\underline{r}_2|_c)}{|\underline{r}_2|_c}\ T_n^1(\hat{\underline{r}}_1\cdot\hat{\underline{r}}_2),\end{aligned} \tag{55}$$

where $T_n^1(x)$ is the Gegenbauer function and

$$\hat{\underline{r}}_i=\frac{\underline{r}_i}{|\underline{r}_i|_c} \quad \text{for} \quad i=1,2, \tag{56}$$

and the integral[12]

$$\lim_{\epsilon'\to 0^+}\int_0^{+\infty} J_\nu(ap)J_\mu(ap)\,\frac{pdp}{p^2-k_0^2-i\epsilon'} = \frac{\pi i}{2}\,J_\mu(ak_0)H_\nu^{(1)}(ak_0), \tag{57}$$

where $\mu\geq\nu$, $\mu-\nu$ is an even integer and $a>0$, to reduce (52) to the form

$$\begin{aligned}\bar{\underline{K}}^{aa}(\underline{k}_1,\underline{k}_2)=\exp[-i(\underline{k}_1-\underline{k}_2)\cdot\underline{d}_1]\Bigg[&\bar{\underline{1}}\epsilon(\epsilon-1)a_1b_1c_1\\ &\times\frac{j_1(|\underline{\underline{K}}_{11}-\underline{\underline{K}}_{21}|_c)}{|\underline{\underline{K}}_{11}-\underline{\underline{K}}_{21}|_c}-\frac{(\epsilon-1)^2}{2\pi^2}\,(a_1b_1c_1)^2\\ &\times\pi ik_0\int_0^1 dx_p\int_0^{2\pi}d\varphi_p(\bar{\underline{1}}-\hat{p}\hat{p})\\ &\times\sum_{\substack{n=0\\ n+m=\text{ even}}}^{\infty}\sum_{m=0}^{\infty}(2n+3)(2m+3)\\ &\times\frac{j_{n+1}(|\underline{\underline{K}}_{11}|_c)}{|\underline{\underline{K}}_{11}|_c}\,\frac{j_{m+1}(|\underline{\underline{K}}_{21}|_c)}{|\underline{\underline{K}}_{21}|_c}\\ &\times\frac{j_{m_>+1}(k_0Y^{aa})h_{m_<+1}(k_0Y^{aa})}{(Y^{aa})^2}\\ &\times T_n^1(\hat{\underline{P}}_1\cdot\hat{\underline{\underline{K}}}_{11})T_m^1(\hat{\underline{P}}_1\cdot\hat{\underline{\underline{K}}}_{21})\Bigg],\end{aligned} \tag{58}$$

where

$$m_>=\max\{m,n\}, \qquad m_<=\min\{m,n\} \tag{59}$$

$$h_n(x)=\left(\frac{\pi}{2x}\right)^{1/2}H_{n+1/2}^{(1)}(x) \quad \text{(spherical Hankel function)}, \tag{60}$$

$$Y^{aa}=(a_1^2Z_x^2+b_1^2Z_y^2+c_1^2Z_z^2)^{1/2}, \tag{61}$$

$$\hat{\underline{\underline{P}}}_1=\frac{1}{Y^{aa}}\,(a_1Z_x,b_1Z_y,c_1Z_z), \tag{62}$$

$$|\underline{\underline{K}}_{11}|_c=n_0k_0(a_1^2H_x^2+b_1^2H_y^2+c_1^2H_z^2)^{1/2}, \tag{63}$$

$$\hat{\underline{\underline{K}}}_{11}=\frac{1}{(a_1^2H_x^2+b_1^2H_y^2+c_1^2H_z^2)^{1/2}}\,(a_1H_x,b_1H_y,c_1H_z), \tag{64}$$

$$|\underline{\underline{K}}_{21}|_c=n_0k_0(a_1^2\Lambda_x^2+b_1^2\Lambda_y^2+c_1^2\Lambda_z^2)^{1/2}, \tag{65}$$

and

$$\hat{\underline{\underline{K}}}_{21}=\frac{1}{(a_1^2\Lambda_x^2+b_1^2\Lambda_y^2+c_1^2\Lambda_z^2)^{1/2}}\,(a_1\Lambda_x,b_1\Lambda_y,c_1\Lambda_z). \tag{66}$$

The dyadic $\bar{\underline{1}}-\hat{p}\hat{p}$ has the representation

$$\bar{\underline{1}}-\hat{p}\hat{p}=\begin{bmatrix}1-y^2\cos^2\varphi_p & -y^2\cos\varphi_p\sin\varphi_p & -xy\cos\varphi_p\\ -y^2\cos\varphi_p\sin\varphi_p & 1-y^2\sin^2\varphi_p & -xy\sin\varphi_p\\ -xy\cos\varphi_p & -xy\sin\varphi_p & y^2\end{bmatrix}, \tag{67}$$

where $y^2=1-x^2$ and $x=\cos\vartheta_p$.

The expression for the matrix element $\bar{\underline{K}}^{bb}(\underline{k}_1,\underline{k}_2)$ is similar and is given in Appendix A.

Now, substituting (28), (29), and (30) into (22) gives

$$\bar{\underline{K}}^{ab}(\underline{k}_1,\underline{k}_2)=-\frac{1}{2\pi^2}\lim_{\epsilon'\to 0^+}\int\frac{d\underline{p}p^2}{p^2-k_0^2-i\epsilon'}\times(\bar{\underline{1}}-\hat{p}\hat{p})U_{V_1}(\underline{k}_1,\underline{p})U_{V_2}(\underline{p},\underline{k}_2). \tag{68}$$

Applying (7), (8), (9), and (10), Eq. (68) becomes

$$\begin{aligned}\bar{\underline{K}}^{ab}(\underline{k}_1,\underline{k}_2)=-\frac{1}{2\pi^2}\lim_{\epsilon'\to 0^+}\int\frac{d\underline{p}p^2}{p^2-k_0^2-i\epsilon'}&\times(\bar{\underline{1}}-\hat{p}\hat{p})\exp[-i(\underline{k}_1-\underline{p})\\ &\cdot\underline{d}_1]U'_{V_1}(\underline{\underline{K}}_{11},\underline{\underline{P}}_1)\exp[-i(\underline{p}-\underline{k}_2)\\ &\cdot\underline{d}_2]U'_{V_2}(\underline{\underline{P}}_2,\underline{\underline{K}}_{22}),\end{aligned} \tag{69}$$

where

$$U'_{V_1}(\underline{\underline{K}}_{11},\underline{\underline{P}}_1)=\int_{V_1}d\xi_1\,\frac{\gamma}{k_0^2}\exp[-i(\underline{\underline{K}}_{11}-\underline{\underline{P}}_1)\cdot\xi_1], \tag{70}$$

$$U'_{V_2}(\underline{\underline{P}}_2,\underline{\underline{K}}_{22})=\int_{V_2}d\xi_2\,\frac{\gamma}{k_0^2}\exp[-i(\underline{\underline{P}}_2-\underline{\underline{K}}_{22})\cdot\xi_2], \tag{71}$$

$$\underline{\underline{K}}_{22}=\underline{k}_2\cdot\bar{\underline{\underline{A}}}_2 \tag{72}$$

and

$$\underline{P}_2=\underline{p}\cdot\bar{A}_2. \tag{73}$$

The $\underline{K}_{22}$ and $\underline{P}_2$ vectors are expressed in the local coordinate system $x_2y_2z_2$. The first Born term $U'_{V_2}(\underline{K}_{12},\underline{K}_{22})$ is given by

$$U'_{V_2}(\underline{K}_{12},\underline{K}_{22})=a_2b_2c_2(\epsilon-1)\ \frac{j_1(|\underline{\underline{K}}_{12}-\underline{\underline{K}}_{22}|_c)}{|\underline{\underline{K}}_{12}-\underline{\underline{K}}_{22}|_c}, \tag{74}$$

for any free vectors $\underline{K}_{12}$ and $\underline{K}_{22}$. The new symbols used are defined as follows.

$$\underline{K}_{12}=n_0k_0(\sqrt{1-x_{k_1}^2}\cos\varphi_{k_1},\sqrt{1-x_{k_1}^2}\sin\varphi_{k_1},x_{k_1})\cdot\bar{A}_2 \equiv n_0k_0(M_x,M_y,M_z), \tag{75}$$

$$\underline{\underline{K}}_{12}=n_0k_0(a_2M_x,b_2M_y,c_2M_z), \tag{76}$$

$$\underline{K}_{22}=n_0k_0(\sqrt{1-x_{k_2}^2}\cos\varphi_{k_2},\sqrt{1-x_{k_2}^2}\sin\varphi_{k_2},x_{k_2})\cdot\bar{A}_2 \equiv n_0k_0(T_x,T_y,T_z) \tag{77}$$

and

$$\underline{\underline{K}}_{22}=n_0k_0(a_2T_x,b_2T_y,c_2T_z). \tag{78}$$

Using (74), Eq. (69) becomes

$$\bar{\underline{K}}^{ab}(\underline{k}_1,\underline{k}_2)=-\frac{1}{2\pi^2}\ a_1b_1c_1a_2b_2c_2(\epsilon-1)^2 \times\exp[-i(\underline{k}_1\cdot\underline{d}_1-\underline{k}_2\cdot\underline{d}_2)] \times\int_{-1}^{+1}dx_p\int_0^{2\pi}d\varphi_p \times\lim_{\epsilon'\to0^+}\int_0^{+\infty}\frac{p^4dp}{p^2-k_0^2-i\epsilon'}\ (\bar{\underline{1}}-\hat{p}\hat{p}) \times\exp[-i(\underline{d}_2-\underline{d}_1)\cdot p\hat{p}] \times\frac{j_1(|\underline{\underline{K}}_{11}-\underline{\underline{P}}_1|_c)}{|\underline{\underline{K}}_{11}-\underline{\underline{P}}_1|_c}\frac{j_1(|\underline{\underline{P}}_2-\underline{\underline{K}}_{22}|_c)}{|\underline{\underline{P}}_2-\underline{\underline{K}}_{22}|_c}, \tag{79}$$

where

$$\underline{P}_2=p(\sqrt{1-x_p^2}\cos\varphi_p,\sqrt{1-x_p^2}\sin\varphi_p,x_p)\cdot\bar{A}_2 \equiv p(\Xi_x,\Xi_y,\Xi_z) \tag{80}$$

and

$$\underline{\underline{P}}_2=p(a_2\Xi_x,b_2\Xi_y,c_2\Xi_z). \tag{81}$$

In order to perform the p-integration, we apply Cauchy's integral formula[11] and then carry out numerical integration.[13] The final form of (79) is the following

$$\begin{aligned}\bar{\underline{K}}^{ab}(\underline{k}_1,\underline{k}_2)=&-\frac{1}{2\pi^2}\ a_1b_1c_1a_2b_2c_2(\epsilon-1)^2\exp[-i(\underline{k}_1\cdot\underline{d}_1-\underline{k}_2\cdot\underline{d}_2)]\Bigg[\int_{-1}^{+1}dx_p\int_0^{2\pi}d\varphi_p\pi i\ \frac{k_0^3}{2}\ (\bar{\underline{1}}-\hat{p}\hat{p})\\ &\times\exp[-i(\underline{d}_2-\underline{d}_1)\cdot k_0\hat{p}]\ \frac{j_1[|\underline{\underline{K}}_{11}-\underline{\underline{P}}_1(k_0)|_c]}{|\underline{\underline{K}}_{11}-\underline{\underline{P}}_1(k_0)|_c}\frac{j_1[|\underline{\underline{P}}_2(k_0)-\underline{\underline{K}}_{22}|_c]}{|\underline{\underline{P}}_2(k_0)-\underline{\underline{K}}_{22}|_c}\\ &+\int_{-1}^{+1}dx_p\int_0^{2\pi}d\varphi_p\int_0^{k_0-\delta}\frac{p^4dp}{p^2-k_0^2}\ (\bar{\underline{1}}-\hat{p}\hat{p})\exp[-i(\underline{d}_2-\underline{d}_1)\cdot p\hat{p}]\ \frac{j_1(|\underline{\underline{K}}_{11}-\underline{\underline{P}}_1|_c)}{|\underline{\underline{K}}_{11}-\underline{\underline{P}}_1|_c}\frac{j_1(|\underline{\underline{P}}_2-\underline{\underline{K}}_{22}|_c)}{|\underline{\underline{P}}_2-\underline{\underline{K}}_{22}|_c}\\ &+\int_{-1}^{+1}dx_p\int_0^{2\pi}d\varphi_p\int_{k_0+\delta}^{+\infty}\frac{p^4dp}{p^2-k_0^2}\ (\bar{\underline{1}}-\hat{p}\hat{p})\exp[-i(\underline{d}_2-\underline{d}_1)\cdot p\hat{p}]\ \frac{j_1(|\underline{\underline{K}}_{11}-\underline{\underline{P}}_1|_c)}{|\underline{\underline{K}}_{11}-\underline{\underline{P}}_1|_c}\frac{j_1(|\underline{\underline{P}}_2-\underline{\underline{K}}_{22}|_c)}{|\underline{\underline{P}}_2-\underline{\underline{K}}_{22}|_c}\Bigg].\end{aligned} \tag{82}$$

The real quantity δ used in the p-integration is positive and $\delta\to0^+$. The expression for $\bar{\underline{K}}^{ba}(\underline{k}_1,\underline{k}_2)$ is obtained in a similar way and is given in Appendix A.

The element $\bar{\underline{J}}_iU_{V_1}(\underline{k}_1,\underline{k}_i)$ of the right part of the matrix equation (27) takes the form

$$\bar{\underline{J}}_iU_{V_1}(\underline{k}_1,\underline{k}_i)=(\bar{\underline{1}}-\hat{k}_i\hat{k}_i)\exp[-i(\underline{k}_1-\underline{k}_i)\cdot\underline{d}_1]a_1b_1c_1(\epsilon-1)\ \frac{j_1(|\underline{\underline{K}}_{11}-\underline{\underline{K}}_{i1}|_c)}{|\underline{\underline{K}}_{11}-\underline{\underline{K}}_{i1}|_c}, \tag{83}$$

where

$$\underline{K}_{i1}=\underline{k}_i\cdot\bar{A}_1=k_0(\sqrt{1-x_{k_i}^2}\cos\varphi_{k_i},\sqrt{1-x_{k_i}^2}\sin\varphi_{k_i},x_{k_i})\cdot\bar{A}_1\equiv k_0(\Sigma_x,\Sigma_y,\Sigma_z) \tag{84}$$

and

$$\underline{\underline{K}}_{i1}=k_0(a_1\Sigma_x,b_1\Sigma_y,c_1\Sigma_z). \tag{85}$$

The expression for $\underline{\bar{J}}_i U_{V_2}(\underline{k}_1, \underline{k}_i)$ is given in Appendix B.

Substituting (17) into (14) gives

$$\underline{\bar{f}}(\underline{k}_s, \underline{k}_i) = k_0^2 \underline{\bar{J}}_s \cdot \int U_{V_1}(\underline{k}_s, \underline{k}_2) \underline{\bar{C}}_1(\underline{k}_2) d\underline{k}_2 + k_0^2 \underline{\bar{J}}_s \cdot \int U_{V_2}(\underline{k}_s, \underline{k}_2) \underline{\bar{C}}_2(\underline{k}_2) d\underline{k}_2 . \quad (86)$$

The integral equation (27) is reduced by quadrature into a set of linear equations (a matrix equation). If we choose the $\underline{k}_2$ pivots and weights to be the set

$$S = \{\underline{\kappa}_j, w_j | j = 1, \ldots, n'\}, \quad (87)$$

the arbitrary $\underline{k}_1$ is restricted to a maximum of n' arbitrary values. We choose these to be those of set S. Then (27) and (86) reduce to the equations

$$\sum_{l=1}^{n'} w_l \begin{bmatrix} \underline{\bar{K}}^{aa}(\underline{\kappa}_j, \underline{\kappa}_l) & \underline{\bar{K}}^{ab}(\underline{\kappa}_j, \underline{\kappa}_l) \\ \underline{\bar{K}}^{ba}(\underline{\kappa}_j, \underline{\kappa}_l) & \underline{\bar{K}}^{bb}(\underline{\kappa}_j, \underline{\kappa}_l) \end{bmatrix} \cdot \begin{bmatrix} \underline{\bar{C}}_1(\underline{\kappa}_l) \\ \underline{\bar{C}}_2(\underline{\kappa}_l) \end{bmatrix} = \begin{bmatrix} \underline{\bar{J}}_i U_{V_1}(\underline{\kappa}_j, \underline{k}_i) \\ \underline{\bar{J}}_i U_{V_2}(\underline{\kappa}_j, \underline{k}_i) \end{bmatrix} \quad j = 1,2, \ldots, n' . \quad (88)$$

and

$$\underline{\bar{f}}(\underline{k}_s, \underline{k}_i) = k_0^2 \underline{\bar{J}}_s \cdot \left[\sum_{l=1}^{n'} w_l \underline{\bar{C}}_1(\underline{\kappa}_l) U_{V_1}(\underline{k}_s, \underline{\kappa}_l) + \sum_{l=1}^{n'} w_l \underline{\bar{C}}_2(\underline{\kappa}_l) U_{V_2}(\underline{k}_s, \underline{\kappa}_l) \right] . \quad (89)$$

The matrix equation (88) is solved by applying the lower-upper matrix (LU) decomposition algorithm.[14] Then the values of $\underline{\bar{C}}_1(\underline{\kappa}_l)$ and $\underline{\bar{C}}_2(\underline{\kappa}_l)$ are substituted into (89) and the scattering amplitude is obtained.

3 COMPUTATION AND CONVERGENCE

3.1 COMPUTATIONAL ASPECTS

Irradiation of an RBC rouleau model, consisting of two oblate spheroidal erythrocytes, by a plane wave of $\lambda = 0.633$ μm (in vacuum) was considered in all numerical computations. Spheroids instead of triaxial ellipsoids (with three different semiaxes) were chosen only for ease of future comparison of FIEM with methods pertaining to axisymmetric scatterers. Such a choice does not necessarily affect the computational demands of the program. The index of refraction of the suspending medium was taken as $n_p = 1.33$,[15] whereas the relative (to the suspending medium) complex index of refraction of each RBC was taken as $n_0 = \sqrt{\epsilon} = 1.04 + i\,10^{-4}$.[16] Therefore the equivolumetric radius of each RBC was $a = 2.780$ μm and the size parameter $k_0 a \cong 36.7$.

Serial and parallel Fortran 77 computer codes were developed and run on the following shared-memory parallel systems: SGI Power Series 4D/480S (8×R3000 processors, 70 Mflops), SGI Challenge XL (16×R4400 processors, 320 Mflops) and SGI Power Challenge XL (14×R8000 processors, 4200 Mflops). Double-precision arithmetic was used throughout the computation. It was noticed that approximately 99% of the total computing time was spent on the calculation of the final matrix elements. Furthermore, the calculation of every matrix element could be performed independently of the calculation of any other matrix element. Thus, parallel processing of the final matrix elements led to a dramatic decrease in the total computing time needed. The speedup achieved depended on both the number of processors used and the overall load of the system during the calculation.

It should be pointed out that scattering in the forward direction and in the near forward angular region is of particular importance to many diagnostic applications, such as the optical quantification of erythrocyte aggregation and sedimentation.[17,18] It has also been experimentally observed that light scattered by individual RBCs is strongly forward peaked.[19] Therefore, we restricted our calculations in the forward and near forward scattering directions. Typical elapsed times for reliable results in this scattering region ranged between 10 and 48 h on the SGI Challenge XL system when six processors were used and the overall load of the machine was medium.

3.2 CONVERGENCE

In order to obtain the scattering diagram [the relative scattered intensity $I = |\underline{f}(\varphi_{k_s} = \text{const.}, \vartheta_{k_s}, \varphi_{k_i}, \vartheta_{k_i}, \varphi_{e_i}, \vartheta_{e_i})|^2$ versus the scattering angle ϑ_{k_s}] in the near-forward angular interval (up to $\pm$ 25 deg around the direction of incidence), the following procedure was applied. For the calculation of the matrix elements $\underline{\bar{K}}^{aa}(\underline{k}_1, \underline{k}_2)$ and $\underline{\bar{K}}^{bb}(\underline{k}_1, \underline{k}_2)$ given in Eqs. (58) and (97), the approximation of truncating the infinite summations at a value $n = m = n\max$ was applied. The number of $\underline{k}_2$ pivot vectors (equal to the number of $\underline{k}_1$ vectors), the number of terms $n\max$ in the summations, and the number of integration intervals in the dx_p, $d\varphi_p$ and dp integrations in Eqs. (58), (82), (97), and (104) were increased until convergence was obtained. Furthermore, the position of the pivot vectors was changed until convergence, with presumably the lowest possible computing cost, was achieved. It was found that pivot vectors forming angles greater than 5 deg with the direction of incidence were of little importance to the near forward scattering diagram. Besides, increasing their number led to a sharp increase in the computing time demands of the model. Thus, care was taken to restrict the number of pivot vectors to the smallest possible value

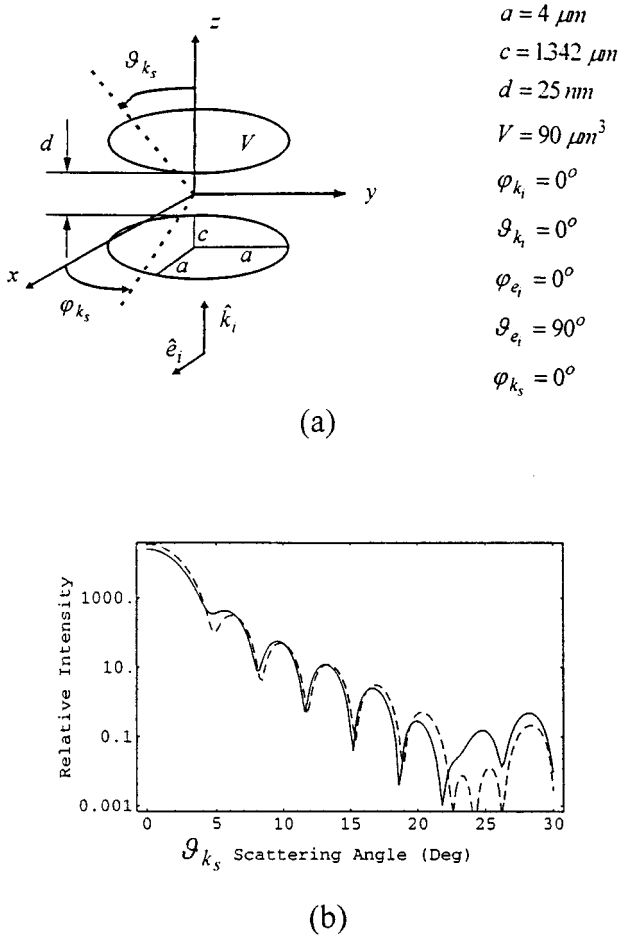

Fig. 2 (a) Irradiation geometry of a model of a two red blood cell rouleau. (b) Near-forward scattering diagrams as predicted by FIEM for coupled scatterers (solid line) and FIEM for the approximate case with the electromagnetic interaction neglected (dashed line). Six pivot vectors were used in both cases.

without losing significant accuracy in the angular region of interest. The values of the above-mentioned discretization parameters generally varied from case to case.

A list of typical values, which proved sufficient in order to achieve convergence for the case depicted in Figure 2(a) (complete analysis), is the following. Six pivot vectors were used: one in the forward direction, four equally spaced around the forward direction and forming an angle of 0.5 deg with it, and one in the backward direction. $n\max=60$ for both $\underline{\bar{K}}^{aa}(\underline{k}_1,\underline{k}_2)$ and $\underline{\bar{K}}^{bb}(\underline{k}_1,\underline{k}_2)$; $\delta=10^{-6}k_0$. $\int_0^1 dx_p$ integration in $\underline{\bar{K}}^{aa}(\underline{k}_1,\underline{k}_2)$ and $\underline{\bar{K}}^{bb}(\underline{k}_1,\underline{k}_2)$: 10 equal subintervals were used. A 16-point Gauss integration was performed on each subinterval.[13] The same algorithm was also applied to each subinterval of all the remaining integrations. $\int_{-1}^{+1} dx_p$ integration in $\underline{\bar{K}}^{ab}(\underline{k}_1,\underline{k}_2)$ and $\underline{\bar{K}}^{ba}(\underline{k}_1,\underline{k}_2)$: 15 equal subintervals were used. $\int_0^{2\pi} d\varphi_p$ integration in $\underline{\bar{K}}^{aa}(\underline{k}_1,\underline{k}_2)$ and $\underline{\bar{K}}^{bb}(\underline{k}_1,\underline{k}_2)$: 20 equal subintervals were used. $\int_0^{2\pi} d\varphi_p$ integration in $\underline{\bar{K}}^{ab}(\underline{k}_1,\underline{k}_2)$ and $\underline{\bar{K}}^{ba}(\underline{k}_1,\underline{k}_2)$: 30 equal subintervals were used. $\int_0^{k_0-\delta} dp$ integration in $\underline{\bar{K}}^{ab}(\underline{k}_1,\underline{k}_2)$ and $\underline{\bar{K}}^{ba}(\underline{k}_1,\underline{k}_2)$: the integration range $[0,k_0-\delta]$ was subdivided into the intervals $[0,k_0-100\delta)$, $[k_0-100\delta,k_0-10\delta]$ and $[k_0-10\delta,k_0-\delta]$. The first interval was further subdivided into three equal subintervals, whereas each one of the last two intervals was considered a single subinterval. $\int_{k_0+\delta}^{+\infty} dp$ integration in $\underline{\bar{K}}^{ab}(\underline{k}_1,\underline{k}_2)$ and $\underline{\bar{K}}^{ba}(\underline{k}_1,\underline{k}_2)$: infinity was satisfactorily replaced by the value of $10k_0$. The resulting integration range $[0,10k_0]$ was subdivided into the intervals $[k_0+\delta,k_0+10\delta)$, $[k_0+10\delta,k_0+100\delta)$, and $[k_0+100\delta,10k_0]$. Each one of the first two intervals was considered a single subinterval. The last interval was subdivided into 27 equal subintervals.

A variable step-length routine that uses a Clenshaw–Curtis quadrature and has a built-in estimate of the absolute error obtained by comparing Newton Cotes and Romberg estimates[20] was alternatively used in some of the previously mentioned integrations.

3.3 COMPARISON WITH MIE THEORY

A partial test of the computer program (adequately modified) was performed by considering the case of plane electromagnetic wave scattering from a single spherical RBC. The scattering amplitude was calculated by applying both the exact Mie theory[21] and the FIEM adequately modified so that it could be used in the single scatterer case. The scattering diagrams for values of ϑ_{k_s} between 0 and 180 deg are given in Ref 22. Six pivot vectors were used in FIEM (one in the forward direction or direction of incidence, four equally spaced around the forward direction and forming an angle of 0.5 deg with it, and one in the backward direction). It has been observed that FIEM compares favorably with Mie theory in the angular interval of up to ± 25 deg around the direction of incidence.[22]

3.4 TEST OF THE PROGRAM FOR THE APPROXIMATE CASE WITH THE ELECTROMAGNETIC INTERACTION NEGLECTED

The program was further tested by considering the approximate case with the electromagnetic interaction neglected ($\underline{\bar{K}}^{ab}(\underline{k}_1,\underline{k}_2)=\underline{\bar{K}}^{ba}(\underline{k}_1,\underline{k}_2)=\underline{\bar{0}}$) and by making use of the following remark. Let $\underline{f}_1(\hat{z},\hat{z})$ be the vector scattering amplitude for the single dielectric ellipsoid shown in Figure 3(a), if the direction of both incidence and scattering is that of $\hat{z}$. The incident wave polarization is taken as $\hat{e}_i=\hat{x}$. Similarly, let $\underline{f}_2(\hat{z},\hat{z})$ be the corresponding vector scattering amplitude for the system of two noninteracting identical ellipsoids shown in Figure 3(b).

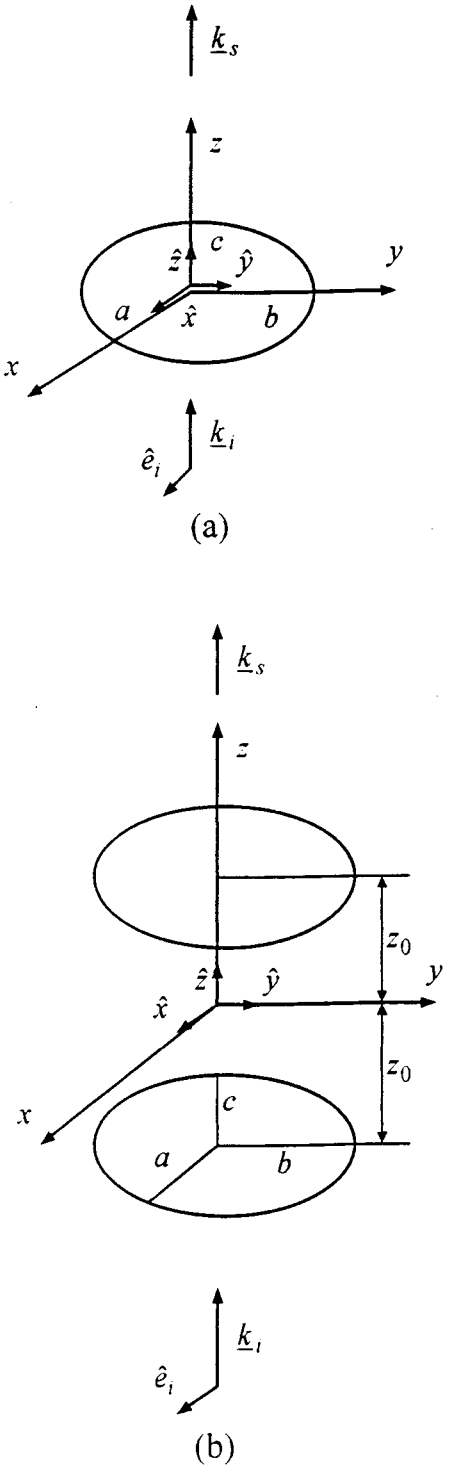

Fig. 3 (a) Irradiation geometry of a single dielectric ellipsoid and (b) of a system of two identical dielectric ellipsoids, used in order to test the FIEM algorithm for the approximate case with the electromagnetic interaction neglected.

According to Eq. (12), the scattered electric field at any point on the positive z axis in the far field and for the first case is given by

$$\underline{E}_1^s(z)=\underline{f}_1(\hat{z},\hat{z})\ \frac{\exp(ik_0z)}{z}, \tag{90}$$

whereas for the second case, it is given by

$$\underline{E}_2^s(z)=\underline{f}_2(\hat{z},\hat{z})\ \frac{\exp(ik_0z)}{z}. \tag{91}$$

The $\underline{E}_2^s(z)$ field may also be expressed as follows (noninteracting scatterers)

$$\underline{E}_2^s(z)=\underline{f}_1(\hat{z},\hat{z})\ \frac{\exp(ik_0|z-z_0|)}{|z-z_0|}\ \exp(ik_0z_0) + \underline{f}_1(\hat{z},\hat{z})\ \frac{\exp(ik_0|z+z_0|)}{|z+z_0|}\ \exp(-ik_0z_0). \tag{92}$$

In the far field, it holds that

$$z\gg z_0. \tag{93}$$

Therefore,

$$\underline{E}_2^s(z)\cong\underline{f}_1(\hat{z},\hat{z})\left[\frac{\exp[ik_0(z-z_0)]}{z}\ \exp(ik_0z_0) + \frac{\exp[ik_0(z+z_0)]}{z}\ \exp(-ik_0z_0)\right]. \tag{94}$$

Consequently,

$$\underline{E}_2^s(z)\cong 2\underline{f}_1(\hat{z},\hat{z})\ \frac{\exp(ik_0z)}{z}. \tag{95}$$

Comparing (91) with (95) gives

$$\underline{f}_2(\hat{z},\hat{z})=2\underline{f}_1(\hat{z},\hat{z}). \tag{96}$$

The vector scattering amplitudes $2\underline{f}_1(\hat{z},\hat{z})$ and $\underline{f}_2(\hat{z},\hat{z})$ were calculated for the case of the oblate spheroidal RBCs of Figure 2(a). The differences between the corresponding vector elements were less than 0.2% when only six pivot vectors were used. Hence, an additional partial check of the program has been provided.

4 NUMERICAL RESULTS

The effect of electromagnetic coupling between two adjacent oblate spheroidal erythrocytes simulating a two red blood cell rouleau is illustrated in Figures 2 and 4. The value of the separation distance between the erythrocytes is a typical value of the distance between the (actually parallel) surfaces of the aggregated cells.[23] It may be noticed that although coupling is substantial when the direction of the wave incidence is parallel to the axis of the aggregate, it is practically insignificant for incidence perpendicular to the axis of the aggregate. This may be attributed to the fact that scattering of red light by erythrocytes is basically forward oriented.[19]

Figures 5 and 6 demonstrate the differences between the near-forward scattering patterns of a single erythrocyte and of a two red blood cell rouleau. Two angles of incidence have been

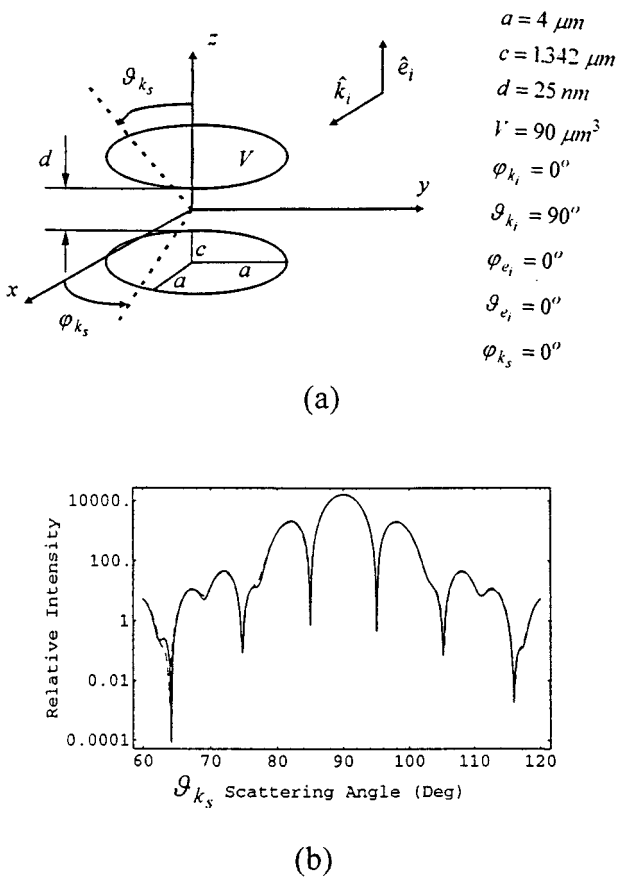

Fig. 4 (a) Irradiation geometry of a model of a two red blood cell rouleau. (b) Comparison between FIEM for coupled scatterers (solid line) and FIEM for the approximate case with the electromagnetic interaction neglected (dashed line). Six pivot vectors were used in both cases.

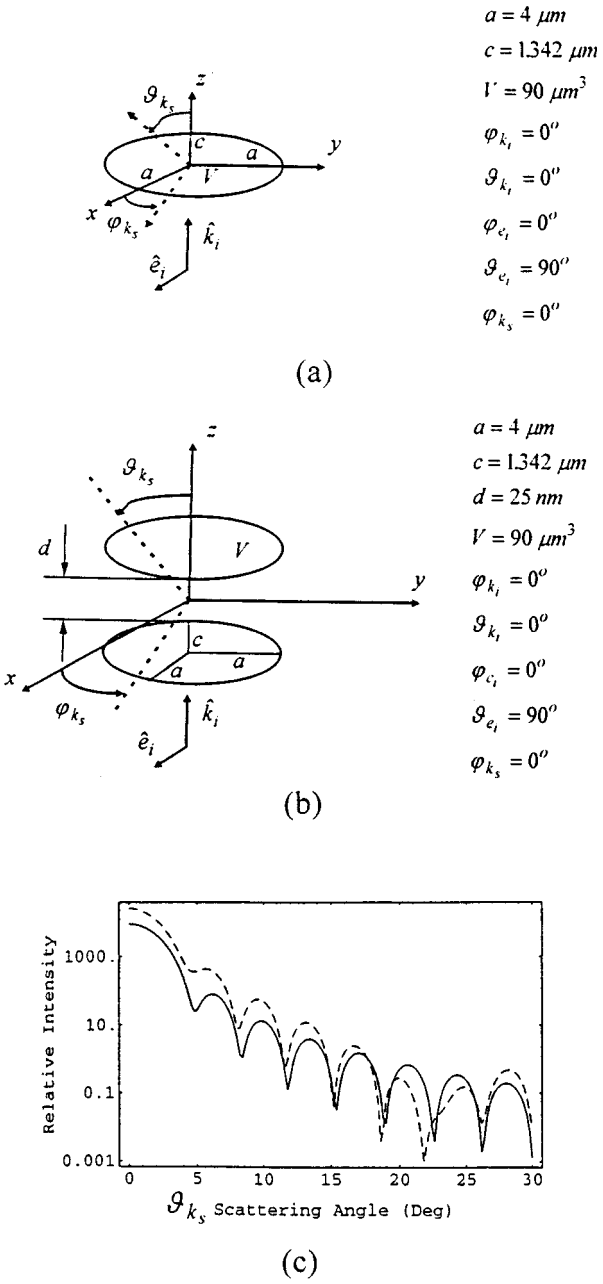

Fig. 5 (a) Irradiation geometry of a single erythrocyte model and (b) of a model of a two red blood cell rouleau. (c) Comparison between their near-forward scattering patterns. Solid line, case (a); dashed line, case (b). Six pivot vectors were used in both cases.

considered. It is evident that easy discrimination between the two cases can be achieved in diagnostic techniques such as flow cytometry,[24] if the near-forward scattering pattern is adequately processed.

5 CONCLUSIONS

A Fredholm integral equation solution to the scattering of a plane electromagnetic wave by a system of two interacting triaxial ellipsoids of complex index of refraction has been developed. Both the position and the orientation of the scatterers are in principle arbitrary. The analysis developed has been tested for certain special configurations of the scatterer system. It has been subsequently applied to the case of plane wave scattering ($\lambda = 0.633\mu$m in vacuum) from a two red blood cell rouleau, immersed in either plasma or an isotonic and optically equivalent suspending medium.

The effect of electromagnetic coupling between adjacent scatterers as well as the effect of the number of scatterers (a single RBC or a RBC doublet) to the near-forward scattering pattern have been quantified and illustrated.

The drawback of the analysis, when applied to large scatterers, is its relatively high computing cost. However, the computing time demands of the model have been substantially decreased partly by adequate selection of the plane waves (pivot vectors) that represent the electric field inside each scatterer, and partly by parallel processing. A particularly interesting application seems to be the modeling of light scattering by rouleaux of tri-

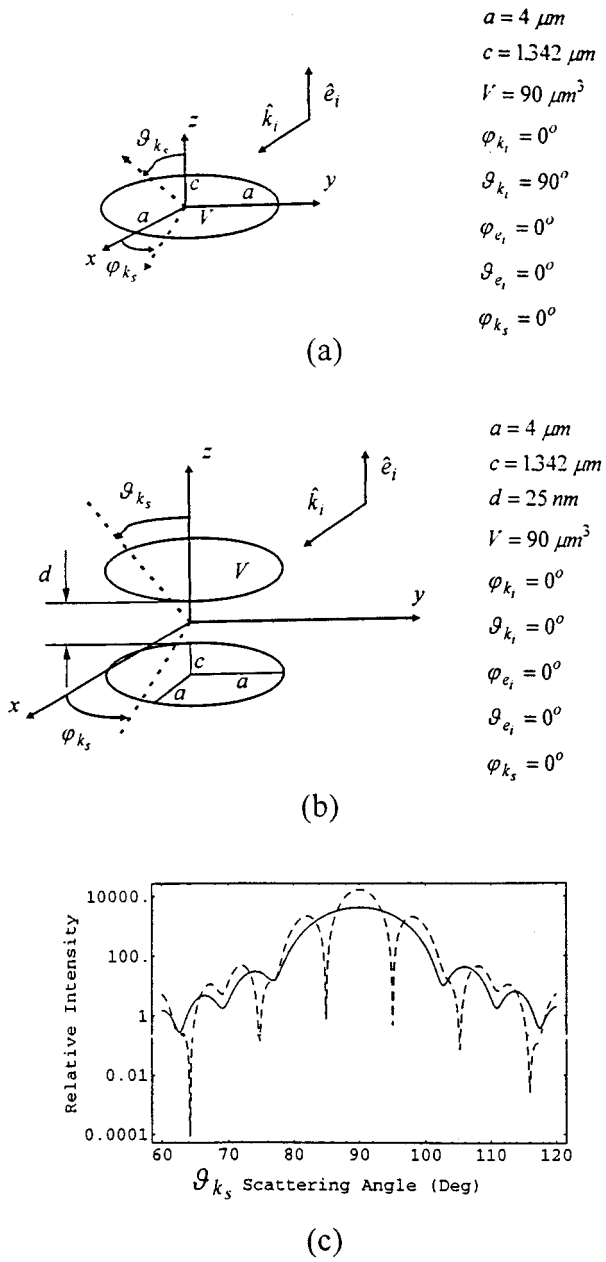

Fig. 6 (a) Irradiation geometry of a single erythrocyte model and (b) of a model of a two red blood cell rouleau. (c) Comparison between their near-forward scattering patterns. Solid line, case (a); dashed line; case (b). Six pivot vectors were used in both cases.

axial elliptocytes, which abound in certain forms of anemia (e.g., elliptocytosis).

6 APPENDIX A

Expressions for the $\bar{\underline{K}}^{bb}(\underline{k}_1,\underline{k}_2)$ and $\bar{\underline{K}}^{ba}(\underline{k}_1,\underline{k}_2)$ matrix elements are as follows:

The matrix element $\bar{\underline{K}}^{bb}(\underline{k}_1,\underline{k}_2)$ has the following expression

$$\bar{\underline{K}}^{bb}(\underline{k}_1,\underline{k}_2)=\exp[-i(\underline{k}_1-\underline{k}_2)\cdot\underline{d}_2]\Bigg[\bar{\underline{1}}\epsilon(\epsilon-1)a_2b_2c_2 \times \frac{j_1(|\underline{\underline{K}}_{12}-\underline{\underline{K}}_{22}|_c)}{|\underline{\underline{K}}_{12}-\underline{\underline{K}}_{22}|_c}-\frac{(\epsilon-1)^2}{2\pi^2} \times(a_2b_2c_2)^2\pi ik_0\int_0^1 dx_p\int_0^{2\pi}d\varphi_p[\bar{\underline{1}}-\hat{p}\hat{p}] \times\sum_{\substack{n=0\\ n+m=\text{ even}}}^{\infty}\sum_{m=0}^{\infty}(2n+3)(2m+3) \times\frac{j_{n+1}(|\underline{\underline{K}}_{12}|_c)}{|\underline{\underline{K}}_{12}|_c}\frac{j_{m+1}(|\underline{\underline{K}}_{22}|_c)}{|\underline{\underline{K}}_{22}|_c} \times\frac{j_{m_>+1}(k_0Y^{bb})h_{m_<+1}(k_0Y^{bb})}{(Y^{bb})^2} \times T_n^1(\hat{\underline{P}}_2\cdot\hat{\underline{\underline{K}}}_{12})T_m^1(\hat{\underline{P}}_2\cdot\hat{\underline{\underline{K}}}_{22})\Bigg], \quad (97)$$

where, by using the symbols introduced in Eqs. (80), (75), and (77),

$$Y^{bb}=(a_2^2\Xi_x^2+b_2^2\Xi_y^2+c_2^2\Xi_z^2)^{1/2}, \quad (98)$$

$$\hat{\underline{P}}_2=\frac{1}{Y^{bb}}\ (a_2\Xi_x,b_2\Xi_y,c_2\Xi_z), \quad (99)$$

$$|\underline{\underline{K}}_{12}|_c=n_0k_0(a_2^2M_x^2+b_2^2M_y^2+c_2^2M_z^2)^{1/2}, \quad (100)$$

$$\hat{\underline{\underline{K}}}_{12}=\frac{1}{(a_2^2M_x^2+b_2^2M_y^2+c_2^2M_z^2)^{1/2}} \times(a_2M_x,b_2M_y,c_2M_z), \quad (101)$$

$$\underline{\underline{K}}|_{22}|_c=n_0k_0(a_2^2T_x^2+b_2^2T_y^2+c_2^2T_z^2)^{1/2} \quad (102)$$

and

$$\hat{\underline{\underline{K}}}_{22}=\frac{1}{(a_2^2T_x^2+b_2^2T_y^2+c_2^2T_z^2)^{1/2}}\ (a_2T_x,b_2T_y,c_2T_z). \quad (103)$$

The expression for the matrix element $\bar{\underline{K}}^{ba}(\underline{k}_1,\underline{k}_2)$ is the following

$$\bar{\underline{K}}^{ba}(\underline{k}_1,\underline{k}_2)=-\frac{1}{2\pi^2}\,a_1b_1c_1a_2b_2c_2(\epsilon-1)^2\,\exp[-i(\underline{k}_1\cdot\underline{d}_2-\underline{k}_2\cdot\underline{d}_1)]\Bigg[\int_{-1}^{+1}dx_p\int_0^{2\pi}d\varphi_p\,\pi i\,\frac{k_0^3}{2}\,(\bar{\underline{1}}-\hat{p}\hat{p})$$

$$\times\exp[i(\underline{d}_2-\underline{d}_1)\cdot k_0\hat{p}]\,\frac{j_1(|\underline{\underline{K}}_{12}-\underline{\underline{P}}_2(k_0)|_c)}{|\underline{\underline{K}}_{12}-\underline{\underline{P}}_2(k_0)|_c}\,\frac{j_1(|\underline{\underline{P}}_1(k_0)-\underline{\underline{K}}_{21}|_c)}{|\underline{\underline{P}}_1(k_0)-\underline{\underline{K}}_{21}|_c}+\int_{-1}^{+1}dx_p\int_0^{2\pi}d\varphi_p\int_0^{k_0-\delta}\frac{p^4dp}{p^2-k_0^2}$$

$$\times(\bar{\underline{1}}-\hat{p}\hat{p})\exp[i(\underline{d}_2-\underline{d}_1)\cdot p\hat{p}]\,\frac{j_1(|\underline{\underline{K}}_{12}-\underline{\underline{P}}_2|_c)}{|\underline{\underline{K}}_{12}-\underline{\underline{P}}_2|_c}\,\frac{j_1(|\underline{\underline{P}}_1-\underline{\underline{K}}_{21}|_c)}{|\underline{\underline{P}}_1-\underline{\underline{K}}_{21}|_c}+\int_{-1}^{+1}dx_p\int_0^{2\pi}d\varphi_p\int_{k_0+\delta}^{+\infty}\frac{p^4dp}{p^2-k_0^2}$$

$$\times(\bar{\underline{1}}-\hat{p}\hat{p})\exp[i(\underline{d}_2-\underline{d}_1)\cdot p\hat{p}]\,\frac{j_1(|\underline{\underline{K}}_{12}-\underline{\underline{P}}_2|_c)}{|\underline{\underline{K}}_{12}-\underline{\underline{P}}_2|_c}\,\frac{j_1(|\underline{\underline{P}}_1-\underline{\underline{K}}_{21}|_c)}{|\underline{\underline{P}}_1-\underline{\underline{K}}_{21}|_c}\Bigg]. \tag{104}$$

7 APPENDIX B

The final expression for the $\bar{\underline{J}}_i U_{V_2}(\underline{k}_1,\underline{k}_i)$ element of the right part of (27) is

$$\bar{\underline{J}}_i U_{V_2}(\underline{k}_1,\underline{k}_i)=(\bar{\underline{1}}-\hat{k}_i\hat{k}_i)\exp[-i(\underline{k}_1-\underline{k}_i)\cdot\underline{d}_2]a_2b_2c_2(\epsilon-1)\,\frac{j_1(|\underline{\underline{K}}_{12}-\underline{\underline{K}}_{i2}|_c)}{|\underline{\underline{K}}_{12}-\underline{\underline{K}}_{i2}|_c}, \tag{105}$$

where

$$\underline{\underline{K}}_{i2}=\underline{k}_i\cdot\bar{\underline{A}}_2=k_0(\sqrt{1-x_{k_i}^2}\cos\varphi_{k_i},\sqrt{1-x_{k_i}^2}\sin\varphi_{k_i},x_{k_i})\cdot\bar{\underline{A}}_2\equiv k_0(\Omega_x,\Omega_y,\Omega_z) \tag{106}$$

and

$$\underline{\underline{K}}_{i2}=k_0(a_2\Omega_x,b_2\Omega_y,c_2\Omega_z). \tag{107}$$

Acknowledgments

We would like to acknowledge the helpfulness of the staff of both the Central and the High Performance Computing Centres of the National Technical University of Athens, where all calculations were performed.

REFERENCES

1. J. P. Barton, S. A. Schaub, and D. R. Alexander, "Electromagnetic field for a beam incident on two adjacent spherical particles," *Appl. Opt.* **30**, 4706–4715 (1991).
2. K. A. Fuller, "Optical resonances and two sphere systems," *Appl. Opt.* **30**, 4716–4731 (1991).
3. M. I. Mishchenko, D. W. Mackowski, and L. D. Travis, "Scattering of light by bispheres with touching and separated components," *Appl. Opt.* **34**, 4589–4599 (1995).
4. S. Nag and B. P. Sinha, "Electromagnetic plane wave scattering by a system of two uniformly lossy dielectric prolate spheroids in arbitrary orientation," *IEEE Trans. Antennas Propagat.* **43**, 322–327 (1995).
5. W. J. Williams, E. Beutler, A. J. Erslev, M. A. Lichtman, *Hematology*, Chaps. 30 and 56, McGraw-Hill, New York (1990).
6. N. K. Uzunoglu and B. G. Evans, "Multiple scattering effects in electromagnetic wave propagation through a medium containing precipitation," *J. Phys. A: Math. Gen.* **41**, 767–776 (1978).
7. N. Uzunoglu, G. Stamatakos, D. Koutsouris, and D. Yova, "Light scattering by adjacent red blood cells—a mathematical model," *Proc. SPIE* **2326**, 334–345 (1994).
8. N. Uzunoglu, "Theoretical Calculations of Scattering of Electromagnetic Waves from Precipitation Particles," PhD Thesis, University of Essex (1976).
9. J. J. Tuma, *Dynamics*, Chap. 9, Quantum Publishers, New York (1974).
10. A. R. Holt, N. K. Uzunoglu, and B. G. Evans, "An integral equation solution to the scattering of electromagnetic radiation by dielectric spheroids and ellipsoids," *IEEE Trans. Antennas Propagat.* **AP-26**, 706–712 (1978).
11. P. M. Morse and H. Feshbach, *Methods of Theoretical Physics*, pp. 473, 1574, McGraw-Hill, New York (1953).
12. G. N. Watson, *A Treatise on the Theory of Bessel Functions*, Chap. 13, p. 429, Cambridge University Press, Cambridge (1966).
13. M. Abramowitz and I. A. Stegun, eds., *Handbook of Mathematical Functions*, pp. 887–888, Dover Publications, New York (1972).
14. W. H. Press, S. A. Teukolsky, W. T. Vetterling, and B. P. Flannery, *Numerical Recipes in Fortran* 2nd ed., Chap. 2, pp. 34–41, Cambridge Univ. Press, Cambridge (1992).
15. R. A. Meyer, "Light scattering from red blood cell ghosts: sensitivity of angular dependent structure to membrane thickness and refractive index," *Appl. Opt.* **16**, 2036–2038 (1977).
16. A. N. Korolevich, A. Ya. Khairullina, and L. P. Shubochkin, "Scattering matrix of a monolayer of optically soft close-packed particles," *Opt. Spectrosc. (USSR)* **68**(2), 236–239 (1990).
17. E. Muralidharan, N. Tateishi, and N. Maeda, "A new laser photometric technique for the measurement of erythrocyte aggregation and sedimentation kinetics," *Biorheology* **31**, 277–285 (1994).
18. E. Muralidharan, "Simultaneous determination of hematocrit, aggregate size and sedimentation velocity by He-Ne laser scattering," *Biorheology* **31**, 587–599 (1994).
19. A. H. Gandjbakhche, P. Mills, and P. Snabre, "Light scattering technique for the study of orientation and deformation of red blood cells in a concentrated suspension," *Appl. Opt.* **33**, 1070–1078 (1994).
20. H. O'Hara and F. J. Smith, "The evaluation of definite integrals by interval subdivision," *Comp. J.* **12**, 179–182 (1969).
21. M. Born and E. Wolf, *Principles of Optics*, Chap. 13.5, pp. 633–664, Pergamon Press, Oxford (1993).
22. G. S. Stamatakos and N. K. Uzunoglu, "An integral equation solution to the scattering of electromagnetic radiation by a linear chain of interacting dielectric ellipsoids. The case of a red blood cell rouleau," *J. Electromagnetic Waves Appl.* **11**, 949–980 (in press) (1997).
23. S. Chien, "Aggregation of red blood cells: an electrochemical and colloid chemical problem," *Adv. Chem. Sci.* **188**, 3–38 (1980).
24. H. M. Shapiro, *Practical Flow Cytometry*, p. 5, Alan R. Liss, New York (1985).